Materials Today Bio 13 (2022) 100180

Contents lists available at ScienceDirect

Materials Today Bio

journal homepage: www.journals.elsevier.com/materials-today-bio

A nanosized anionic MOF with rich thiadiazole groups for controlled oral drug delivery

Ke Jiang [a,c], Weishu Ni [a], Xianying Cao [a], Ling Zhang [b,*], Shiwei Lin [b,**]

[a] Key Laboratory of Food Nutrition and Functional Food of Hainan Province, School of Food Science and Engineering, Hainan University, Haikou, 570228, China
[b] State Key Laboratory of Marine Resource Utilization in South China Sea, School of Materials Science and Engineering, Hainan University, Haikou, 570228, China
[c] State Key Laboratory of Silicon Materials, Zhejiang University, Hangzhou, 310027, China

ARTICLE INFO

Keywords:
metal-Organic framework
Controlled drug delivery
Surface engineering
Crystal size control

ABSTRACT

Controlling the crystal size and surface chemistry of MOF materials, and understanding their multifunctional effect are of great significance for the biomedical applications of MOF systems. Herein, we designed and synthesized a new anionic MOF, ZJU-64-NSN, which features 1D channels decorated with highly polarized thiadiazole groups, and its crystal size could be systematically tuned from 200 μm to 300 nm through a green and simple approach. As a result, the optimal nanosized ZJU-64-NSN is found to enable an ultrafast loading of cationic drug procainamide (PA) (21.2 wt% within 1 min). Moreover, the undesirable chemical stability of PA@ZJU-64-NSN is greatly improved by the surface coating of polyethylene glycol (PEG) biopolymer. The final drug delivery system PEG/PA@ZJU-64-NSN is found to effectively prevent PA from premature release under the harsh stomach environments due to the intense host-guest interaction, and mainly release PA to the targeted intestinal surroundings. Such controlled drug delivery is proved to be triggered by endogenic Na^+ ions instead of H^+ ions, well revealed by the study on the dynamics behavior of drug release and UV–Vis absorption spectrum. Good biocompatibility of ZJU-64-NSN and PEG-coated ZJU-64-NSN has been fully demonstrated by MTT assay as well as confocal microscopy imaging.

1. Introduction

Procainamide (PA), one of the most helpful antiarrhythmic medications [1], is mainly administered by injection or oral delivery. However, some adverse effects such as infection, hypotension and even shock are very likely to occur if PA is adopted via injection. In addition, quite a few patients suffer from the fear of injection. By enabling painless self-administration, oral delivery is much more preferred way due to its convenience, light patient compliance and cost-effectiveness. Actually, PA holds the short half-life period and must be dosed every 3–4 h [2,3]. High dose of oral PA is often associated with nausea, vomiting and diarrhoea. Most importantly, developments of oral PA delivery have been seriously hindered by the gastrointestinal (GI) tract challenge [4]. PA via individual oral is generally degraded under the harsh gastric environments thereby limiting its transport across the intestinal epithelium into the bloodstream. Advancing efforts dedicated to developing desired drug carriers thus aim to achieve safe and controlled oral PA delivery.

Microporous metal-organic frameworks (MOFs) are a novel class of hybrid functional materials, self-assembled from various organic linkers and metal ions/clusters. The modular nature of MOFs endows them with powerful tunability of pore structure and chemistry, thus popularizing their applications including gas separation [5], [-8] sensing [9–12] and catalysis [13,14]. Particularly, tremendous potentials of MOF materials have been exhibited as drug carriers [15–26] since MIL-101 was explored for the first time in 2006 by Ferey and co-workers [27]. Growing evidence has shown that the properties of MOFs highly depend on their crystal size and surface functionalities [28,29]. In fact, extensive researches have focused on nanosized MOF materials, and the results indicate that nanoparticles can accelerate adsorption/desorption kinetics and improve bioavailability relative to their bulk counterparts [30,31]. Moreover, particles less than 1 μm in size could be transcytosed better by cells [32]. Unfortunately, it is still great challenging for some potential MOFs used for drug carriers, like bio-MOF series [33], to obtain the crystal material with nanoscale size.

Additionally, specific functionalization is one of the most important steps for tuning the properties of MOFs which determines the success in

* Corresponding author.
** Corresponding author.
E-mail addresses: ling.zhang@hainanu.edu.cn (L. Zhang), linsw@hainanu.edu.cn (S. Lin).

https://doi.org/10.1016/j.mtbio.2021.100180
Received 2 November 2021; Received in revised form 30 November 2021; Accepted 2 December 2021
Available online 2 December 2021

their applications to a great degree [34–36]. The primary barrier for oral drug carriers is to achieve the fast loading with high drug capacity. There are two general methods for MOFs to encapsulate cargos. One is one-pot synthesis, applying to some MOFs grown at room temperature like ZIF-8,[37] otherwise the activity of drugs might be affected at too high synthesis temperature. The other is universal immersing method, which is generally time-consuming for most MOFs. For example, it takes 15 days for PA to be encapsulated into bio-MOF-1,[38] and 6 days for Ibuprofen to be loaded into MOF-74-Fe(III) [39]. It is thus of practical significance to explore the feasibility of fast drug loading upon MOF carriers. PA commonly used as its hydrochloride, is one kind of cationic drug, and conventionally time-consuming for encapsulation within neutral MOFs by reason of their weak host-guest interaction. By contrast, anionic MOFs seem to enable the fast PA loading driven by strong electrostatic affinity. In addition, GI challenge is another barrier for oral drug delivery that oral drug need be prevented by nano carriers from degradation in the harsh gastric environments and further be mainly assimilated in intestinal surroundings [40]. But in fact, the chemical stability of most MOF carriers is inadequate in the harsh stomach environments, let alone the achievement of controlled PA release [41,42]. Taken together, it reveals a daunting challenge but necessary to achieve desired oral PA delivery.

In this work, we successfully designed and synthesized a new anionic MOF, ZJU-64-NSN, isostructural to ZJU-64-CH_3, which features 1D channels decorated with rich highly polarized thiadiazole groups. The crystal size of ZJU-64-NSN could be systematically tuned from 200 μm to 300 nm through a green and simple approach named thermal-stirring method. As a result, the anionic network of nanosized ZJU-64-NSN lined by rich thiadiazole groups enables an ultrafast cationic PA loading (21.2 wt% within 1 min), thus revealing the practical significance of ZJU-64-NSN as a drug carrier. Moreover, the undesirable chemical stability of PA@ZJU-64-NSN has been greatly improved after the post-modification by the nontoxic and nonimmunogenic polyethylene glycol (PEG) biopolymer. The optimal delivery system PEG/PA@ZJU-64-NSN is found to effectively prevent PA from early release under the simulated stomach environments with the presence of stomach acid and pepsin, and finally release PA under the simulated physiological conditions (Scheme 1). The dynamics study on drug release behavior reveals the mechanism of controlled PA release is mainly due to the ion exchange with endogenic Na^+ ions instead of H^+ ions. Apart from that, good biocompatibility of ZJU-64-NSN and PEG-coated ZJU-64-NSN has been fully demonstrated by MTT assay as well as confocal microscopy imaging.

2. Experimental section

2.1. Synthesis routes to the organic linker H_2BTDBA

Synthesis of dimethyl 4,4'-(benzo[c][1,2,5]thiadiazole-4,7-diyl) dibenzoate (2): 4,7-dibromo-4,7-dihydrobenzo [c][1,2,5]thiadiazole (4.4 g, 15 mmol), 1 (14.41 g, 45 mmol), K_2CO_3 (27.8 g, 200 mmol) were mixed in 1,4-dioxane (100 mL) and the mixture was stirred for half an hour at room temperature purging with argon meantime. After that, $Pd(PPh_3)_2Cl_2$ (0.3 g, 0.4 mmol) was added and then the mixture was stirred at 85 °C for 3 d under argon. The resultant mixture was extracted with $CHCl_3$ and water three times after the reaction was cooled down. Anhydrous $MgSO_4$ was used for drying the organic phase and the organic phase was removed under reduced pressure. The crude product was purified with toluene recrystallization to obtain the pure dimethyl 4,4'-(benzo[c][1,2,5]thiadiazole-4,7-diyl)dibenzoate (2). Yield: 2.5 g. Synthesis of 4,4'-(benzo[c][1,2,5]thiadiazole-4,7-diyl)dibenzoic acid (3): The product dimethyl 4,4'-(benzo[c][1,2,5]thiadiazole-4,7-diyl)dibenzoate (2) (1 g, 2.5 mmol) was suspended in a mixture of 100 mL of 10 M NaOH aqueous solution and THF (20 mL). The mixture was stirred under reflux overnight and the THF was removed under reduced pressure. The pH value of the mixture was adjusted to 3 by Dilute HCl. The solid was collected by filtration, washed with water until the pH value up to 7, and dried at 65 °C to get H_2BTDBA. Yield: 0.8 g (85%); ^{1}H NMR (500 MHz, DMSO), δ = 8.06 (s, 2H), 8.10 (d, 4H), 8.15 (d, 4H).

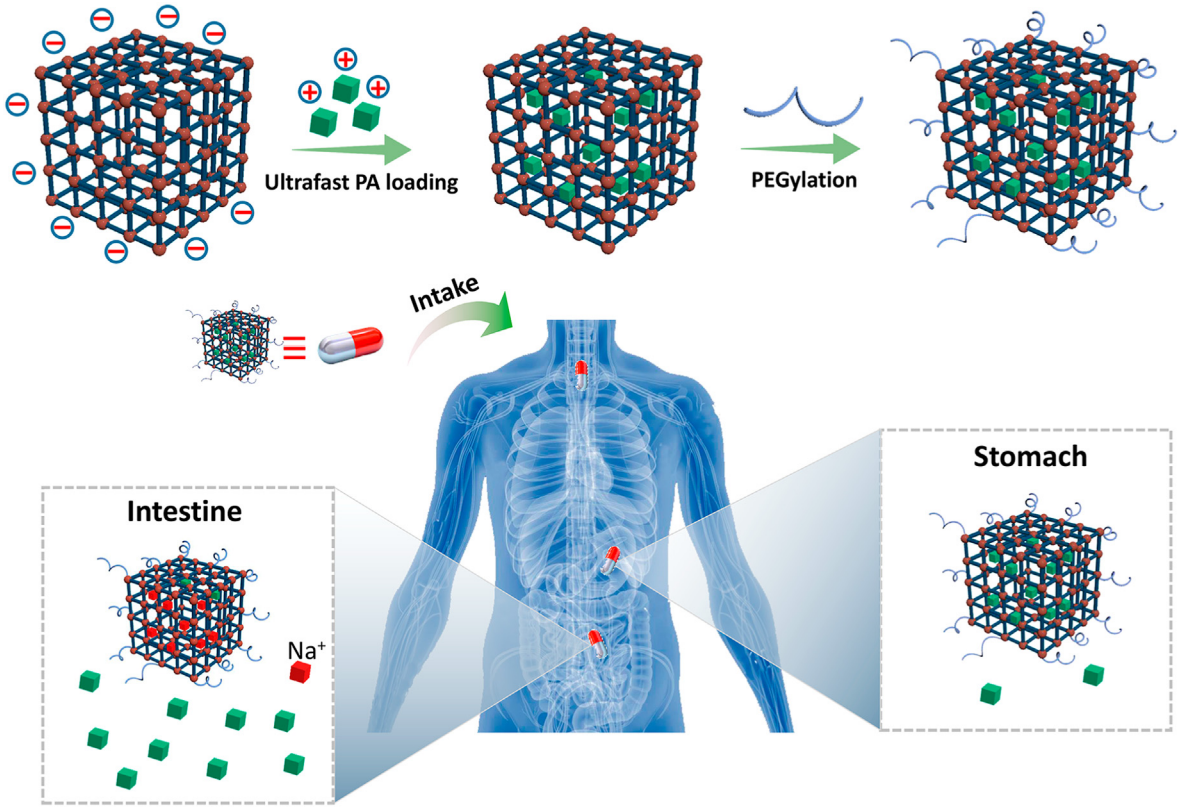

Scheme 1. Synthesis of PEG/PA@ZJU-64-NSN and PA controlled delivery.

2.2. Size controlled of ZJU-64-NSN

2.2.1. Synthesis of ZJU-64-NSN (200 μm)

28 mg of H_2BTDBA, 8 mg of adenine and 73 mg of $Zn(NO_3)_2{\cdot}6H_2O$ were mixed into the DMF solution (12 mL) as well as the deionized water (1 mL) and nitric acid (40 μL). The mixed solution were ultrasonic mixing uniformly. The resulting solution was heated at 130 °C for 24 h. After the mixture was cooled and washed with fresh DMF, yellow crystals were obtained as ZJU-64-NSN.

2.2.2. Synthesis of ZJU-64-NSN (4 μm)

28 mg of H_2BTDBA, 8 mg of adenine and 73 mg of $Zn(NO_3)_2{\cdot}6H_2O$ were mixed into the DMF solution (12 mL) as well as the deionized water (1.1 mL) and nitric acid (40 μL). The mixed solution was ultrasonic mixing uniformly and stirred at 130 °C for 24 h. The resulting yellow powder was collected by centrifugation at 13,000 rpm for 10 min and washed with DMF and methanol three times. The yellow powder was soaking in DMF and methanol overnight and then dried at 60 °C to get the dried powder.

2.2.3. Synthesis of ZJU-64-NSN (1 μm)

28 mg of H_2BTDBA, 8 mg of adenine and 219 mg of $Zn(NO_3)_2{\cdot}6H_2O$ were mixed into the DMF solution (12 mL) as well as the deionized water (1 mL) and nitric acid (40 μL). The mixed solution was ultrasonic mixing uniformly and stirred at 130 °C for 24 h. The resulting yellow powder was collected by centrifugation at 13,000 rpm for 10 min and washed with DMF and methanol three times. The yellow powder was soaking in DMF and methanol overnight and then dried at 60 °C to get the dried powder.

2.2.4. Synthesis of ZJU-64-NSN (300 nm)

28 mg of H_2BTDBA, 8 mg of adenine and 292 mg of $Zn(NO_3)_2{\cdot}6H_2O$ were mixed into the DMF solution (12 mL) as well as the deionized water (1 mL) and nitric acid (40 μL). The mixed solution was ultrasonic mixing uniformly and stirred at 130 °C for 24 h. And the resulting yellow powder was collected by centrifugation at 13,000 rpm for 10 min and washed with DMF and methanol three times. The yellow powder was soaking in DMF and methanol overnight and then dried at 60 °C to get the dried powder.

2.3. Encapsulation of drug procainamide hydrochloride (PA)

The PA was encapsulated into the ZJU-64-NSN (300 nm) by immersing 20 mg of ZJU-64-NSN into 10 mL of deionized water PA solution (20 mg mL^{-1}) at room temperature under stirring for 1 min, 30 min and 24 h. The PA loaded ZJU-64-NSN (PA@ZJU-64-NSN) was collected by centrifugation at 10,000 rpm for 10 min. And PA@ZJU-64-NSN was washed three times with water and dried in the vacuum oven. The drug loading capacity was measured by ^{1}H NMR spectroscopy.

2.4. Decoration of PA@ZJU-64-NSN with mPEG-NH_2

40 mg of mPEG-NH_2 (M_n = 5000) was dissolved in 4 mL methanol (anhydrous, 99.8%). 30 mg PA@ZJU-64-NSN was dispersed into the above solution under stirring. Once PA@ZJU-64-NSN and mPEG-NH_2 were mixed, stirring was terminated. The solution was standing at 37 °C for 24 h, and the samples were collected by centrifugation, washed several times with water and methanol, and dried overnight at room temperature to obtain PEG/PA@ZJU-64-NSN.

3. Results and discussion

3.1. Structural characterization of ZJU-64-NSN

The organic linker 4,4'-(benzo[c][1,2,5]thiadiazole-4,7-diyl)dibenzoic acid (H_2BTDBA) was synthesized via Suzuki coupling, followed by hydrolysis and acidification, as shown in Fig. 1a and Figure S1. Reaction H_2BTDBA (Fig. 1c) and adenine with $Zn(NO_3)_2{\cdot}6H_2O$ afforded yellow bulk crystals ZJU-64-NSN. The powder purity of ZJU-64-NSN was obtained by powder X-ray diffraction analysis, suggesting that the structure of ZJU-64-NSN is isostructural to the series of.

ZJU-64 (Fig. 2b) [43–45]. The zinc-adenine cluster (Fig. 1b) interconnect with multiple $BTDBA^{2-}$ linkers to form the three-dimensional (3D) framework of ZJU-64-NSN (Fig. 1d). Most importantly, 1D channels of ZJU-64-NSN are decorated with highly polarized thiadiazole groups running along c axis with a size of about ~12.2 Å × 12.2 Å, quite suitable for the further encapsulation of PA (Figure S3) [46].

3.2. Size-controlled synthesis of ZJU-64-NSN

In order to make a desired drug carrier, it is strongly recommended for downsizing the crystal of ZJU-64-NSN from millimeter scale to nanoscale, but quite difficult for well size-control of such complex MOF systems [47]. To overcome such difficulties, a convenient method called heat-stirring synthesis via accelerating the nucleation rate was attempted to tune the crystal size of ZJU-64-NSN. Finally, by introducing agitation during the crystal nucleation and growth, we successfully well-control the crystal size of ZJU-64-NSN from 200 μm to 5 μm along with a satisfactory rectangular morphology, evidenced by scanning electron microscope (SEM) images (Fig. 2a). The crystal size of ZJU-64-NSN was further reduced from 5 μm to 300 nm by increasing the proportion of Zn^{2+} (Fig. 2a), which probably because the nucleation rate of ZJU-64-NSN was accelerated. Moreover, PXRD analysis reveals that ZJU-64-NSN with various crystal sizes holds the same structure, as revealed by their same patterns observed in Fig. 2b. The nanosized crystal of ZJU-64-NSN (~300 nm) was further verified by dynamic light scattering (DLS) in Figure S4, and such desired nanosized MOF was employed for subsequent study of drug loading and delivery.

3.3. Ultrafast drug loading properties of nanosized ZJU-64-NSN

Encouraged by the anionic framework lined by highly polarized thiadiazole groups, appropriate pore volume and nanosized particle of ZJU-64-NSN, we first evaluate its drug loading kinetics behavior of a cationic model drug PA. Before cargo encapsulation, the as-synthesized ZJU-64-NSN was exchanged sufficiently by DMF and methanol successively to remove the unreacted organic ligand. Then, the drug encapsulation procedure was proceeded in aqueous solution of PA with vigorous stirring for 1 min, 30 min, and 24 h respectively. ^{1}H NMR analyses indicate that the PA loading capacities of ZJU-64-NSN are almost equal up to 0.21 g/g regardless of 24 h, 0.5 h or 1 min (Figure S6-S8), revealing the cationic drug PA encapsulation within ZJU-64-NSN can fast reach the saturation within 1 min. Such fast drug loading along with moderately high cargo capacity suggests the very promising drug carrier of ZJU-64-NSN among ever reported MOF drug carriers (Table S2) [37–39,48]. The diffraction peak positions of PXRD pattern remain almost unchanged before and after the PA encapsulation (Fig. 2b), indicating the structural integrity of MOF could be held during the PA loading process. Moreover, the Fourier transform infrared (FTIR) spectrum analysis (Fig. 2c) shows that the characteristics bimodal bands at 3401.2 and 3321.1 cm^{-1}, attributed to the $-NH_2$ stretching vibration of PA were observed in ZJU-64-NSN after PA loading. Besides, the Brunauer-Emmett-Teller (BET) surface area of ZJU- 64-NSN decreased from 945 m^2 g^{-1} to 7 m^2 g^{-1} after PA loading (Fig. 3a). These results further confirmed the successful encapsulation of PA within ZJU-64-NSN.

3.4. Surface modification of PA@ZJU-64-NSN with PEG polymer

In addition to the drug loading ability, the drug delivery needs nanocarriers to bear a desired chemical stability under the biorelevant conditions [49]. We thus explore the chemical stability of PA@ZJU-64-NSN in simulated physiological conditions

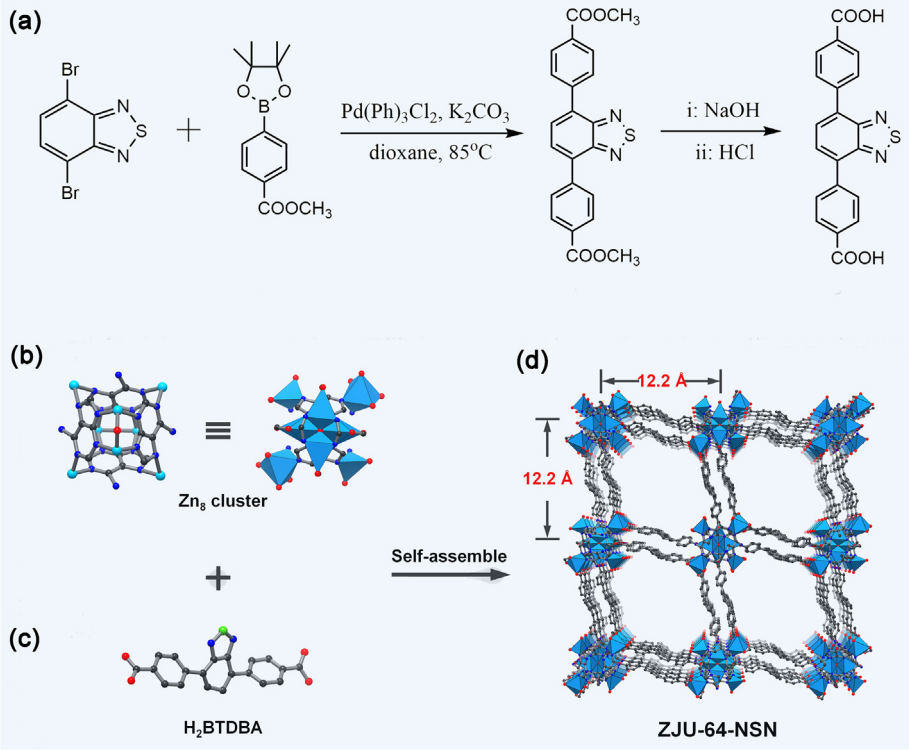

Fig. 1. (a) Synthetic routes to the organic linker H_2BTDBA. Crystal structure of ZJU-64-NSN: (b) the Zn_8 cluster; (c) the organic linker H_2BTDBA; (d) the 1D pore channels with a size of about ~12.2 Å × 12.2 Å viewed from the c axis (C, dark gray; O, red; Zn, cambridge blue; N, blue; S, green; H atoms are omitted for the clarity).

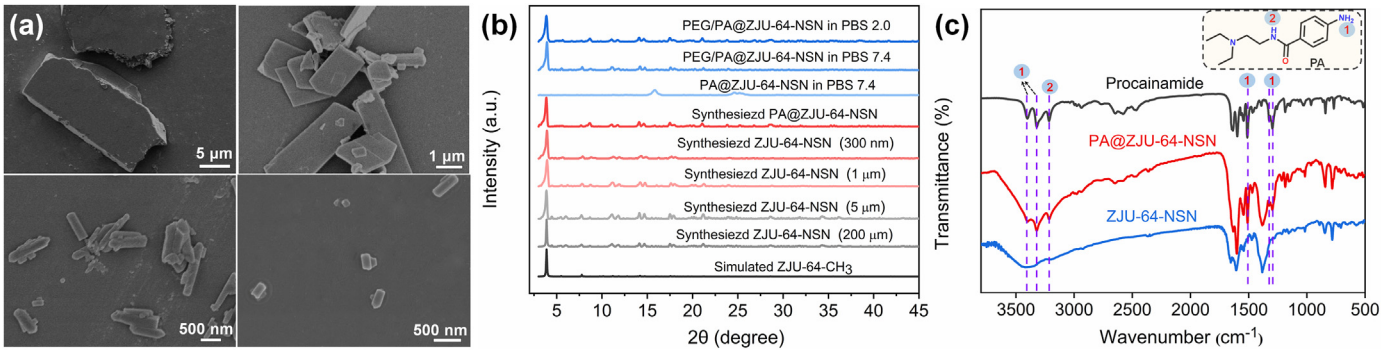

Fig. 2. (a) SEM images of ZJU-64-NSN with particle size of 200 μm, 5 μm, 1 μm and 300 nm. (b) PXRD patterns of ZJU-64-NSN samples with different sizes; PA@ZJU-64-NSN and PEG/PA@ZJU-64-NSN after immersing in PBS 7.4 and 2.0 for overnight. (c) FTIR spectra of ZJU-64-NSN, PA@ZJU-64-NSN, and procainamide.

(phosphate-buffered saline also known as PBS solution with pH 7.4 at 37 °C). As shown in Fig. 2b, PXRD analyses indicate that PA@ZJU-64-NSN seriously degrade after soaking in such conditions for overnight, likely as a consequence of the exchange of the organic linker with phosphates [50]. It thus reveals the inadequate chemical stability of PA@ZJU-64-NSN for further oral PA delivery. Modifying the surface of drug carriers with nontoxic and nonimmunogenic biopolymers like PEG series is the most commonly method to protect NPs from premature clearance [51–55]. We describe the surface coating of mPEG-NH_2 onto PA@ZJU-64-NSN through a green functionalization process. The presence of PEG coating was direct evidenced by FTIR analysis. The characteristic adsorption bands at 2885 and 1115 cm^{-3} attributed to the –O-CH_3 and -C-O-C-stretching vibrations from free PEG were observed in PEG coated PA@ZJU-64-NSN with a slight shift, but not found in uncoated PA@ZJU-64-NSN, thus confirming the successful PEG coating (Fig. 3b) [55]. Interestingly, PA@ZJU-64-NSN after the PEG coating clearly show an improved chemical stability relative to uncoated PA@ZJU-64-NSN, as evidence by PXRD analyses (Fig. 2b), in which PEG/PA@ZJU-64-NSN remain stable even under PBS solution (pH 2.0) for overnight. Such results confirm the good chemical stability of PEG/PA@ZJU-64-NSN thanks to the shielding effect of PEG coating [53], thus satisfying the stability requirement of nanocarriers for the oral drug delivery.

3.5. *Controlled drug delivery properties and mechanism of PEG/PA@ZJU-64-NSN*

The sustained PA release behavior at 37 °C from PEG/PA@ZJU-64-NSN were investigated in PBS solutions at pH 7.4 and 2.0 respectively, and the release profiles were measured by using Ultraviolet–visible (UV–vis) method. Clearly, the release of PA from PEG/PA@ZJU-64-NSN was effectively inhibited at pH 2.0, as shown in Fig. 3c, with only ~20% of amount was detected after sustained release 50 h. Conversely, it significantly accelerated when pH value was increased to 7.4, and over 70% PA was released just after 10 h, exhibiting a “hypothetical” reverse pH- controlled drug delivery. To further confirm the mechanism of PA

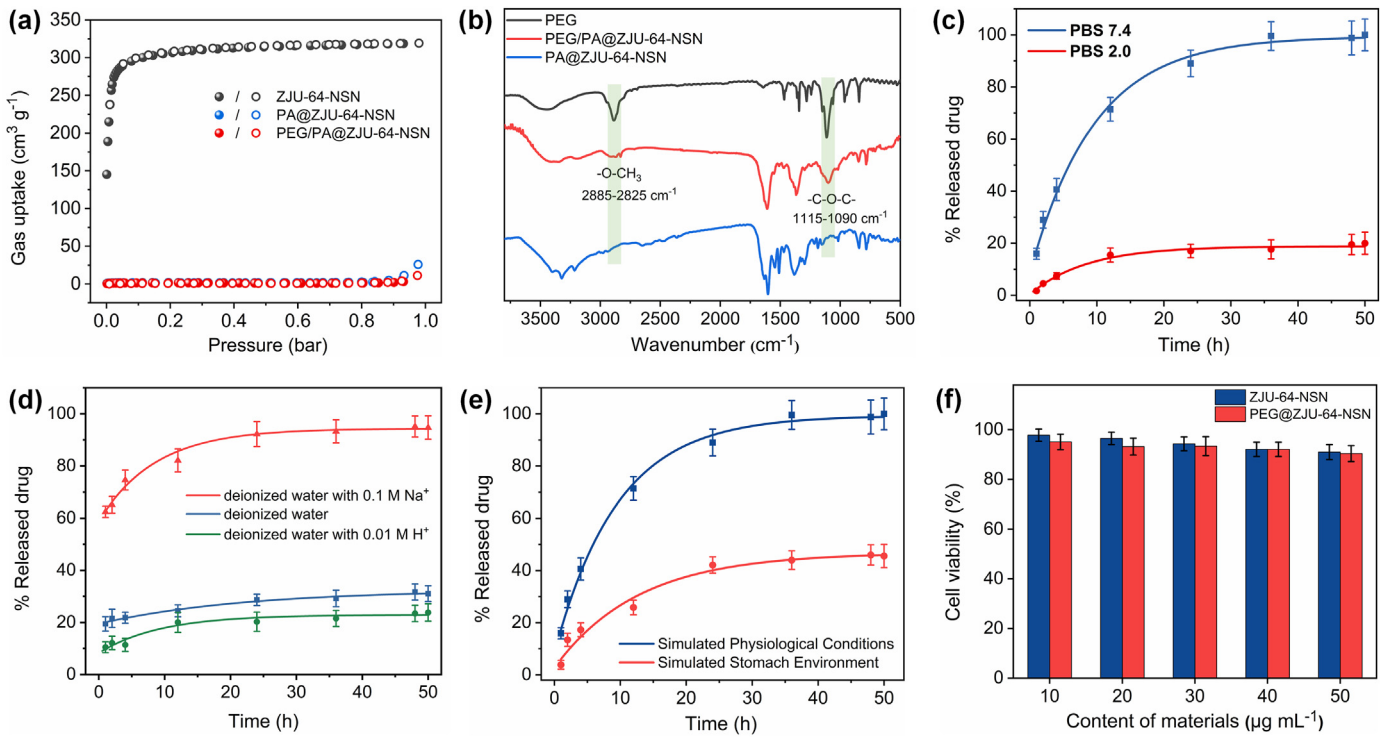

Fig. 3. (a) The N_2 adsorption isotherms at 77 K of ZJU-64-NSN, PA@ZJU-64-NSN and PEG/PA@ZJU-64-NSN. (b) FTIR spectra of PEG, PEG/PA@ZJU-64-NSN, and PA@ZJU-64-NSN. (c) Drug release profile of PEG/PA@ZJU-64-NSN in PBS 7.4 and 2.0. (d) Drug release mechanism of PEG/PA@ZJU-64-NSN. (e) Drug release profile of PEG/PA@ZJU-64-NSN in gastrointestinal simulation fluid. (f) MTT assay of ZJU-64-NSN and PEG@ZJU-64-NSN.

release from PEG/PA@ZJU-64-NSN, we accordingly conducted the release experiments in deionized water solutions of relevant pH values configured by hydrochloric acid (Fig. 3d). Unexpectedly, there was only slight amount of PA detected and no apparent difference was observed in both deionized water solution with or without 0.01 M H^+, thus revealing H^+ could not trigger the release of PA from PEG/PA@ZJU-64-NSN. Actually, it is not difficult to understand that there are strong host-guest interactions between cationic PA and anionic MOF framework. Moreover, such strong interaction would be further strengthened due to the protonation of PA in more acidic conditions, verified by.

UV–Vis spectrum analyses of PA in various PBS solutions (Figure S9). In other words, the interaction between PA and ZJU-64-NSN would be enhanced with the concentration increase of H^+, further restraining PA release within the anionic MOF framework. We thus further explore other potential factors that could trigger the release of PA from PEG/PA@ZJU-64-NSN. It is worth noting that the significant difference of PBS solutions at pH 7.4 and 2.0 is not only the concentration of H^+, but also the concentration of Na^+. Actually, PBS solution at pH 2.0 features the low Na^+ concentration (~0.006 M) while over 0.1 M (~0.14 M) concentration of Na^+ is observed in PBS solution at pH 7.4 [56]. As far as we know, other metal cation such as K^+ in PBS do not have such significant concentration differences between pH 7.4 and pH 2.0. Hence, Na^+ aqueous solution was selected for further explore the PA delivery mechanism. As expected, over 80% PA was rapidly released from PEG/PA@ZJU-64-NSN in aqueous solution with 0.1 M Na^+ after 10 h, further confirming the release of PA is mainly attributed to Na^+ ion. Such controlled release is very likely driven by cation exchange due to the moderate size of Na^+ and stronger host-guest interaction.

Considering the barrier of harsh stomach environments is not limited to the gastric acid, pepsin might also hinder the oral PA delivery [57]. A simulated stomach solution (gastric acid and pepsin included) was thus employed to evaluate the PA release of PEG/PA@ZJU-64-NSN. As shown in Fig. 3e, relative to the accelerated cargo release in simulated physiological condition, the low amount of released PA after exposure to such harsh stomach conditions further demonstrates the intense host-guest interaction. The study on dynamics behavior of drug release has well demonstrated the desired oral drug carrier of PEG-coated ZJU-64-NSN, overall consideration of the protect ability of cationic drug in stomach and the motivation effect of drug release to the target intestine position.

3.6. *Biocompatibility of PEG-coated and uncoated ZJU-64-NSN*

In view of biological applications, the cytotoxicity of ZJU-64-NSN carrier and the impact of PEG coating on cell toxicity of ZJU-64-NSN carrier were further evaluated by means of thiazolyl blue tetrazolium bromide (MTT) assay [58]. Rat pheochromocytoma (PC12) cells were selected here as a commonly employed cellular model for the incubation with ZJU-64-NSN and PEG-coated ZJU-64-NSN with various concentration of 10 and 50 μg mL^{-1} for sustainable 24 h. As illustrated in Fig. 3f, the cell viability is higher than 90% even at 50 μg mL^{-1} dose of ZJU-64-NSN, thereby excluding any adverse effect for the cytotoxicity of such nanosized MOF carrier. Particularly, almost no significant differences in cell viability were observed between the PEG-coated and uncoated ZJU-64-NSN, thus exhibiting the good biocompatible and nontoxic impact of PEG coating. Apart from MTT assay, confocal microscopy was selected for the cytotoxicity visualization based on the enriched neuritis of PC12 cells. The microtubular cytoskeleton (red) and the nuclei (blue) were stained by tubulin and 4,6-diamidino-2-phenylic-dole (DAPI).

Accordingly. The morphology of individual PC12 cells, PC12 cells incubating with ZJU-64-NSN and PEG-coated ZJU-64-NSN at both 50 μg mL^{-1} was shown in Fig. 4. As expected, the appreciable neuritis extension of live PC12 cells convincingly indicated the negligible cytotoxicity and good biocompatibility of ZJU-64-NSN and PEG-coated ZJU-64-NSN.

4. Conclusions

In summary, we have demonstrated the successful design and synthesis of a new anionic MOF ZJU-64-NSN to achieve the controlled cationic drug delivery. The drug loading results indicated the saturation

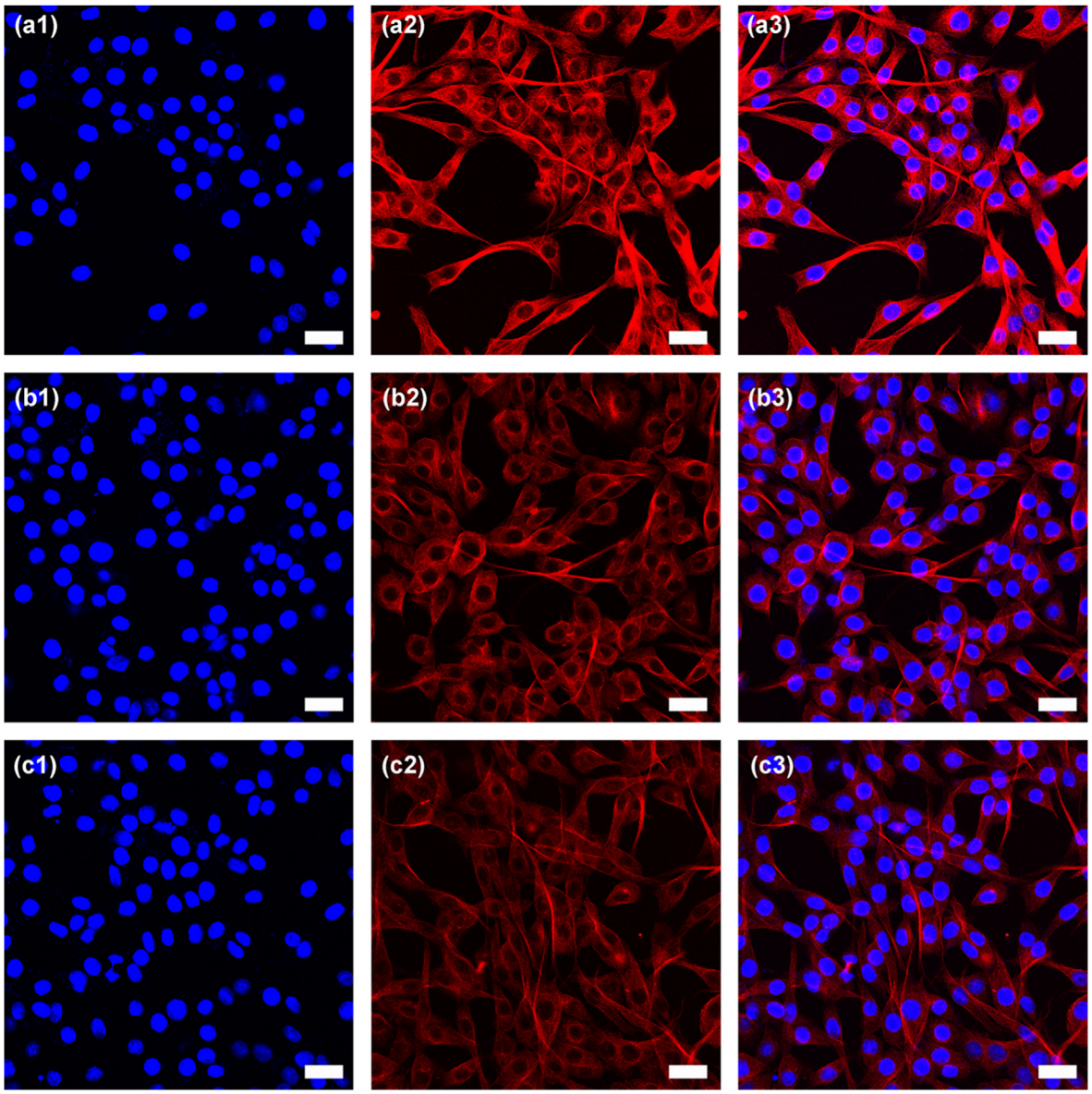

Fig. 4. Confocal microscopy images of individual PC12 cells (a1, a2, and a3), PC12 cells incubated with ZJU-64-NSN (b1, b2, and b3) and PEG-coated ZJU-64-NSN (c1, c2, and c3) with the concentration of 50 μg mL^{-1} for incubation 24 h. Fluorescence field for a1, a2, b1, b2, c1, and c2 overlapped for a3, b3, and c3. Microtubular cytoskeleton (tubulin, red) and nuclei (DAPI, blue) were stained, respectively. Scale bar, 20 μm.

cationic drug PA encapsulation could be ultrafast achieved within such anionic MOF network decorated by polarized thiadiazole groups. Further, the surface coating of PEG remarkably improves the chemical stability of PA@ ZJU-64-NSN when facing the GI tract. Most importantly, PA encapsulated within PEG/PA@ZJU-64-NSN was effectively inhibited from premature release under the simulated stomach environments, and triggered by endogenic Na^+ ions to release under the targeted intestinal surroundings. Good biocompatibility of ZJU-64-NSN and PEG-coated ZJU-64-NSN has been fully demonstrated by MTT assay as well as confocal microscopy imaging. Ultrafast drug loading, excellent chemical stability, good biocompatibility as well as the controlled drug delivery make PEG-coated ZJU-64-NSN a very powerful oral drug carrier. Our work here not only reports the construction of a nanosized MOF material, but offers the approach of using the surface engineering in the functionalization of MOF carrier for particular oral drug delivery.

Credit author statement

Ke Jiang: Investigation, Experiments design & synthesis, Data Formal analysis, Writing – original draft. **Weishu Ni:** Experiments synthesis, Data Formal analysis. **Xianying Cao:** Supervision. **Ling Zhang:** Data Formal analysis, Supervision, Writing – review & editing. **Shiwei Lin:** Supervision, Writing – review & editing.

Declaration of competing interest

The authors declare that they have no known competing financial interests or personal relationships that could have appeared to influence the work reported in this paper.

Acknowledgments

This work was financially supported by the Program of Hainan Association for Science and Technology Plans to Youth R&D Innovation (No. QCXM202002); the National Natural Science Foundation of China (No. 52003069); the National Key R&D Program of China (No. 2017YFC1103800); the Natural Science Foundation of China in Hainan Provincial (No. 520QN221); the Education Department of Hainan

Province (No. Hnky2021ZD-2); and the State Key Laboratory of Advanced Technology for Materials Synthesis and Processing in Wuhan University of Technology (No. 2021-KF-14).

Appendix A. Supplementary data

Supplementary data to this article can be found online at https://doi.org/10.1016/j.mtbio.2021.100180.

References

[1] B. Yang, R. Abel, A. Uprichard, J. Smithers, S. Forgue, Pharmacokinetic and pharmacodynamic comparisons of twice daily and four times daily formulations of procainamide in patients with frequent ventricular premature depolarization, J. Clin. Pharmacol. 36 (1996) 623–633.

[2] J. Koch-Weser, S. Klein, Procainamide dosage schedules, plasma concentrations, and clinical effects, Jama 215 (1971) 1454–1460.

[3] T. Kolettis, N. Kazakos, C. Katsouras, D. Niokou, L. Pappa, V. Koulouras, P. Stefanou, C. Seferiadis, V. Malamou-Mitsi, L. Michalis, M. Marselos, D. Sideris, Intrapericardial drug delivery: pharmacologic properties and long-term safety in swine, Int. J. Cardiol. 99 (2005) 415–421.

[4] F. Benyettou, N. Kaddour, T. Prakasam, G. Das, S. Sharma, S. Thomas, F. Bekhti-Sari, J. Whelan, M. Alkhalifah, M. Khair, H. Traboulsi, R. Pasricha, R. Jagannathan, N. Mokhtari-Soulimane, F. Gandara, A. Trabolsi, In vivo oral insulin delivery via covalent organic frameworks, Chem. Sci. 12 (2021) 6037–6047.

[5] Y. Yang, L. Li, R. Lin, Y. Ye, Z. Yao, L. Yang, F. Xiang, S. Chen, Z. Zhang, S. Xiang, B. Chen, Ethylene/Ethane separation in a stable hydrogen-bonded organic framework through a gating mechanism, Nat. Chem. (2021), https://doi.org/10.1038/s41557-021-00740-z.

[6] L. Zhang, L. Li, E. Hu, L. Yang, K. Shao, L. Yao, K. Jiang, Y. Cui, Y. Yang, B. Li, B. Chen, G. Qian, Boosting ethylene/ethane separation within copper (I)-chelated metal-organic frameworks through tailor-made aperture and specific π-complexation, Adv. Sci. 7 (2020) 1901918.

[7] X. Zhang, L. Li, J. Wang, H. Wen, R. Krishna, H. Wu, W. Zhou, Z. Chen, B. Li, G. Qian, B. Chen, Selective ethane/ethylene separation in a robust microporous hydrogen-bonded organic framework, J. Am. Chem. Soc. 142 (2019) 633–640.

[8] L. Zhang, K. Jiang, L. Yang, L. Li, E. Hu, L. Yang, K. Shao, H. Xing, Y. Cui, Y. Yang, B. Li, B. Chen, G. Qian, Benchmark C_2H_2/CO_2 separation in an ultramicroporous metal-organic framework via copper (I)-alkynyl chemistry, Angew. Chem. Int. Ed. 133 (2021) 16131–16138.

[9] Y. Cui, J. Zhang, H. He, G. Qian, Photonic functional metal-organic frameworks, Chem. Soc. Rev. 47 (2018) 5740–5785.

[10] D. Yue, Y. Wang, D. Chen, Z. Wang, Solvent triggering structural changes for two terbium-based metal-organic frameworks and their photoluminescence sensing, Chem. Commun. 56 (2020) 4320–4323.

[11] J. Zhang, E. Hu, F. Liu, H. Li, T. Xia, Growth of robust metal-organic framework films by spontaneous oxidation of a metal substrate for NO_2 sensing, Mater. Chem. Front. 5 (2021) 6476–6484.

[12] C. Gogoi, A. Kumar, M. SK, S. Biswas, Specific fluorescence sensing of hydrogen sulphide by an azide functionalized Zr(IV) MOF with DUT-52 topology, Microporous Mesoporous Mater. 311 (2021) 110725.

[13] M. Rivera-Torrente, L. Mandemaker, M. Filez, G. Delen, B. Seoane, F. Meirer, B. Weckhuysen, Spectroscopy, microscopy, diffraction and scattering of archetypal MOFs: formation, metal sites in catalysis and thin films, Chem. Soc. Rev. 49 (2020) 6694–6732.

[14] A. Dhakshinamoorthy, A. Asiri, H. Garcia, 2D metal-organic frameworks as multifunctional materials in heterogeneous catalysis and electro/photocatalysis, Adv. Mater. 31 (2019) 1900617.

[15] Y. Bai, Y. Dou, L.-H. Xie, W. Rutledge, J.-R. Li, H.-C. Zhou, Zr-based metal-organic frameworks: design, synthesis, structure, and applications, Chem. Soc. Rev. 45 (2016) 2327–2367.

[16] W. Liu, Y. Pan, Y. Zhong, B. Li, Q. Ding, H. Xu, Y. Qiu, F. Ren, B. Li, M. Muddassir, J. Liu, A multifunctional aminated UiO-67 metal-organic framework for enhancing antitumor cytotoxicity through bimodal drug delivery, Chem. Eng. J. 412 (2021) 127899.

[17] W. Liu, Q. Yan, X. Chen, X. Wang, A. Kumar, Y. Wang, Y. Liu, Y. Pan, J. Liu, Recent advances in cell membrane coated metal-organic frameworks (MOFs) for tumor therapy, J. Mater. Chem. B 9 (2021) 4459–4474.

[18] A. Dutta, Y. Pan, J. Liu, A. Kumar, Multicomponent isoreticular metal-organic frameworks: principles, current status and challenges, Coord. Chem. Rev. 445 (2021) 214074.

[19] Y. Pan, Z. Luo, X. Wang, Q. Chen, J. Chen, Y. Guan, D. Liu, H. Xu, J. Liu, A versatile and multifunctional metal-organic framework nanocomposite toward chemo-photodynamic therapy, Dalton Trans. 49 (2020) 5291–5301.

[20] X. Huang, S. Yu, Y. Wang, X. Jin, B. Wang, L. Gao, H. Zhu, W. Lin, J. Chen, A Y(III)-based metal-organic framework as a carrier in chemodynamic therapy, Inorg. Chem. 59 (2020) 17276–17281.

[21] S. Yu, W. Lin, X. Huang, X. Jin, S. Yao, B. Wang, H. Zhu, J. Chen, A theranostic Mn-based metal-organic framework for T1-weighted magnetic resonance property and chemodynamic therapy, Polyhedron 205 (2021) 115278.

[22] K. Lu, T. Aung, N. Guo, R. Weichselbaum, W. Lin, Nanoscale metal-organic frameworks for therapeutic, imaging, and sensing applications, Adv. Mater. 30 (2018) 1707634.

[23] M. Teplensky, M. Fantham, P. Li, T. Wang, J. Mehta, L. Young, P. Moghadam, J. Hupp, O.K. Farha, C. Kaminski, D. Fairen-Jimenez, Temperature treatment of highly porous zirconium-containing metal-organic frameworks extends drug delivery release, J. Am. Chem. Soc. 139 (2017) 7522–7532.

[24] M. Wang, D. Wang, Q. Chen, C. Li, Z. Li, J. Lin, Recent advances in glucose-oxidase-based nanocomposites for tumor therapy, Small 15 (2019) 1903895.

[25] Y. Liu, C. Gong, L. Lin, Z. Zhou, Y. Liu, Z. Yang, Z. Shen, G. Yu, Z. Wang, S. Wang, Y. Ma, W. Fan, L. He, G. Niu, Y. Dai, X. Chen, Core-shell metal-organic frameworks with fluorescence switch to trigger an enhanced photodynamic therapy, Theranostics 9 (2019) 2791–2799.

[26] S. Gao, P. Zheng, Z. Li, X. Feng, W. Yan, S. Chen, W. Guo, D. Liu, X. Yang, S. Wang, X.-J. Liang, J. Zhang, Biomimetic O_2-evolving metal-organic framework nanoplatform for highly efficient photodynamic therapy against hypoxic tumor, Biomaterials 178 (2018) 83–94.

[27] P. Horcajada, C. Serre, M. Vallet-Regí, M. Sebban, F. Taulelle, G. Férey, Metal-organic frameworks as efficient materials for drug delivery, Angew. Chem. Int. Ed. 118 (2006) 6120–6124.

[28] T. Simon-Yarza, A. Mielcarek, P. Couvreur, C. Serre, Nanoparticles of metal-organic frameworks: on the road to in vivo efficacy in biomedicine, Adv. Mater. 30 (2018) 1707365.

[29] M. Wu, Y. Yang, Metal-organic framework (MOF)-based drug/cargo delivery and cancer therapy, Adv. Mater. 29 (2017) 1606134.

[30] A. Neves, M. Lúcio, S. Martins, J. Lima, S. Reis, Novel resveratrol nanodelivery systems based on lipid nanoparticles to enhance its oral bioavailability, Int. J. Nanomed. 8 (2013) 177–187.

[31] W. Cai, C. Chu, G. Liu, Y. Wang, Metal-organic framework-based nanomedicine platforms for drug delivery and molecular imaging, Small 11 (2015) 4806–4822.

[32] L. Ensign, R. Cone, J. Hanes, Oral drug delivery with polymeric nanoparticles: the gastrointestinal mucus barriers, Adv. Drug Deliv. Rev. 64 (2012) 557–570.

[33] T. Li, M. Kozlowski, E. Doud, M. Blakely, N. Rosi, Stepwise ligand exchange for the preparation of a family of mesoporous MOFs, J. Am. Chem. Soc. 135 (2013) 11688–11691.

[34] Z. Wang, Q. Sun, B. Liu, Y. Kuang, A. Gulzar, F. He, S. Gai, P. Yang, J. Lin, Recent advances in porphyrin-based MOFs for cancer therapy and diagnosis therapy, Coord. Chem. Rev. 439 (2021) 213945.

[35] P. Gao, Y. Chen, W. Pan, N. Li, Z. Liu, B. Tang, Antitumor agents based on metal-organic frameworks, Angew. Chem. Int. Ed. 60 (2021) 16763–16776.

[36] X. Gao, R. Cui, G. Ji, Z. Liu, Size and surface controllable metal-organic frameworks (MOFs) for fluorescence imaging and cancer therapy, Nanoscale 10 (2018) 6205–6211.

[37] H. Zheng, Y. Zhang, L. Liu, W. Wan, P. Guo, A. Nystrom, X. Zou, One-pot synthesis of metal-organic frameworks with encapsulated target molecules and their applications for controlled drug delivery, J. Am. Chem. Soc. 138 (2016) 962–968.

[38] J. An, S. Geib, N. Rosi, Cation-triggered drug release from a porous zinc-adenine metal-organic framework, J. Am. Chem. Soc. 131 (2009) 8376–8377.

[39] Q. Hu, J. Yu, M. Liu, A. Liu, Z. Dou, Y. Yang, A low cytotoxic cationic metal-organic framework carrier for controllable drug release, J. Med. Chem. 57 (2014) 5679–5685.

[40] A. Banerjee, J. Qi, R. Gogoi, J. Wong, S. Mitragotri, Role of nanoparticle size, shape and surface chemistry in oral drug delivery, J. Contr. Release 238 (2016) 176–185.

[41] K. Suresh, A. Matzger, Enhanced drug delivery by dissolution of amorphous drug encapsulated in a water unstable metal-organic framework (MOF), Angew. Chem. Int. Ed. 58 (2019) 16790–16794.

[42] M. Ding, X. Cai, H. Jiang, Improving MOF stability: approaches and applications, Chem. Sci. 10 (2019) 10209–10230.

[43] W. Lin, Q. Hu, J. Yu, K. Jiang, Y. Yang, S. Xiang, Y. Cui, Y. Yang, Z. Wang, G. Qian, Low cytotoxic metal-organic frameworks as temperature-responsive drug carriers, Chem. Plus Chem. 81 (2016) 804–810.

[44] Q. Zhang, M. Wahiduzzaman, S. Wang, S. Henfling, N. Ayoub, E. Gkaniatsou, F. Nouar, C. Sicard, C. Martineau, Y. Cui, G. Maurin, G. Qian, C. Serre, Multivariable sieving and hierarchical recognition for organic toxics in nonhomogeneous channel of MOFs, Inside Chem. 5 (2019) 1337–1350.

[45] H. Wen, L. Li, R. Lin, B. Li, B. Hu, W. Zhou, J. Hu, B. Chen, Fine-tuning of nano-traps in a stable metal-organic framework for highly efficient removal of propyne from propylene, J. Mater. Chem. 6 (2018) 6931–6937.

[46] R. Drout, L. Robison, O. Farha, Catalytic applications of enzymes encapsulated in metal-organic frameworks, Coord. Chem. Rev. 381 (2019) 151–160.

[47] J. Park, Q. Jiang, D. Feng, L. Mao, H.-C. Zhou, Size-controlled synthesis of porphyrinic metal-organic framework and functionalization for targeted photodynamic therapy, J. Am. Chem. Soc. 138 (2016) 3518–3525.

[48] P. Horcajada, C. Serre, G. Maurin, N. Ramsahye, F. Balas, M. Vallet-Regi, M. Sebban, F. Taulelle, G. Ferey, Flexible porous metal-organic frameworks for a controlled drug delivery, J. Am. Chem. Soc. 130 (2008) 6774–6780.

[49] A. Lay, O. Sheppard, C. Siefe, C. Mclellan, R. Mehlenbacher, S. Fischer, M. Goodman, J. Dionne, Optically robust and biocompatible mechanosensitive upconverting nanoparticles, ACS Cent. Sci. 5 (2019) 1211–1222.

[50] X. Li, L. Lachmanski, S. Safi, S. Sene, C. Serre, J.-M. Greneche, J. Zhang, R. Gref, New insights into the degradation mechanism of metal-organic frameworks drug carriers, Sci. Rep. 7 (2017) 13142.

[51] P. Horcajada, T. Chalati, C. Serre, B. Gillet, C. Sebrie, T. Baati, J. Eubank, D. Heurtaux, P. Clayette, C. Kreuz, J. Chang, Y. Hwang, V. Marsaud, P. Bories, L. Cynober, S. Gil, G. Ferey, P. Couvreur, R. Gref, Porous metal-organic-framework nanoscale carriers as a potential platform for drug delivery and imaging, Nat. Mater. 9 (2010) 172–178.

[52] K.E. deKrafft, W. Boyle, L. Burk, O. Zhou, W. Lin, Zr-and Hf-based nanoscale metal-organic frameworks as contrast agents for computed tomography, J. Mater. Chem. 22 (2012) 18139–18144.

[53] I. Lazaro, S. Haddad, S. Sacca, C. Orellana-Tavra, D. Fairen-Jimenez, R. Forgan, Selective surface PEGylation of UiO-66 nanoparticles for enhanced stability, cell uptake, and pH-responsive drug delivery, Inside Chem. 2 (2017) 561–578.
[54] Y. Gu, M. Huang, W. Zhang, M. Pearson, J. Johnson, PolyMOF nanoparticles: dual roles of a multivalent polyMOF ligand in size control and surface functionalization, Angew. Chem. Int. Ed. 131 (2019) 16829–16834.
[55] M. Gimenez-Marques, E. Bellido, T. Berthelot, T. Simon-Yarza, T. Hidalgo, R. Simon-Vazquez, A. Gonzalez-Fernandez, J. Avila, M. Asensio, R. Gref, P. Couvreur, C. Serre, P. Horcajada, GraftFast surface engineering to improve MOF nanoparticles furtiveness, Small 14 (2018) 1801900.
[56] Y. Zheng, J. Sun, X. Jin, X. Wu, Influence of ionic strength on the pH-sensitive in vitro ibuprofen release from dextran-poly (acrylic acid) copolymer, Indian J. Pharmaceut. Sci. 80 (2018) 298–306.
[57] Y. Chen, P. Li, J. Modica, R. Drout, O. Farha, Acid-resistant mesoporous metal-organic framework toward oral insulin delivery: protein encapsulation, protection, and release, J. Am. Chem. Soc. 140 (2018) 5678–5681.
[58] J. Meerloo, G. Kaspers, J. Cloos, Cell sensitivity assays: the MTT assay, Methods Mol. Biol. 1743 (2011) 237–245.